Available online at www.sciencedirect.com

ScienceDirect

Energy Procedia 54 (2014) 310 – 319

Energy Procedia

4th International Conference on Advances in Energy Research 2013, ICAER 2013

# Nudged-Elastic Band Study of Lithium Diffusion in Bulk Silicon in the Presence of Strain

Paramita Haldar[a] and Abhijit Chatterjee[a*]

[a] *Department of Chemical Engineering, Indian Institute of Technology Bombay, Mumbai – 400076,India*

**Abstract**

We study the effect of strain on the lithium diffusion barrier in diamond cubic Si using nudged-elastic band (NEB) method. The modified embedded atom method (MEAM) interatomic potential is employed to describe the interactions between Li and Si atoms. The activation barrier and minimum energy path is found to change significantly as the biaxial strain changes from compressive to tensile in nature. The local strain arising from the presence of neighboring Li atoms is found to affect the activation barrier even more. The Si-Si bond stretching and breaking events during Li diffusion are investigated to elucidate the change in barrier with changing local environment and strain. This study highlights that bulk strain as well as local strain arising from the presence of Li atoms in the vicinity of a diffusing Li atom can affect the Li diffusion constant by orders of magnitude.



Selection and peer-review under responsibility of Organizing Committee of ICAER 2013

*Keywords:* Batteries; lithium; silicon; minimum energy path; elastic strain; transport of Li

## 1. Introduction

An ideal lithium ion battery (LIB) anode material should meet several requirements, such as high capacity for Li, a low potential with respect to the cathode, long cycle life, low cost and environmentally safety [1, 2]. Si is considered as a promising LIB anode material because of its high energy-storage capacity. Si has a theoretical specific capacity of 4200 $mAhg^{-1}$ which is nearly 10 times larger than that of graphite. Such large specific capacities result in larger specific energy densities. In addition, Si is relatively inexpensive due to its abundance on earth and a reasonably low potential. The main issue with use of silicon anodes in LIB is the large volume expansion in Si of up to nearly 400% during lithium insertion [3-6]. This results in fracture due to the formation of an unstable solid electrolyte interphase (SEI) growth on the Si surface [7, 8], loss of electrical contact between the active material and current collector, and pulverization or amorphization of the anode material. In order to mitigate some of these effects, research groups have attempted structural modification of Si in the form of nano-crystals [9], nanowires [10], nanotubes [11], core-shell nanofibers [12, 13], nanoporous materials [14], nanospheres [15], and Si/carbon or

* Corresponding Author, Tel.: +91 (22) 2576 7242; fax: +91 (22) 2572 6895
*E-mail Address:* abhijit@che.iitb.ac.in


Selection and peer-review under responsibility of Organizing Committee of ICAER 2013
doi:10.1016/j.egypro.2014.07.274

Si/graphene nanocomposites [16, 17], which allows for volume expansion with reduced mechanical damage to the anode material. It is known that strain can affect diffusion in solid state materials, i.e., the lithiation/delithiation rates can change as the strain changes. However, the effect of strain on Li diffusion in Si is still poorly understood.

Experimentally, it is known that phase transitions occur in Li-Si alloy during Li insertion as the Li composition changes. Consequently, the electrochemical performance of the anodes also change charge/discharge cycles. Molecular simulations are required to develop an understanding of the mechanisms of Li insertion/extraction with composition, diffusion pathways undertaken by the Li as it is diffused, effect of strain on Li diffusion process, and the role of molecular interactions between Li and Si atoms on the diffusion. There have been a number of theoretical studies in the past on electronic properties [18-20], surface effects [21, 22] of Li-Si alloys, stresses generated during Li insertion [23-31], volume expansion due to Li insertion [32, 33], formation of Li-Si alloys during Li insertion [34-45], and calculation of binding energy at different insertion position and diffusion pathway [45]. However, none of these studies have carefully investigated the effect of strain on the Li diffusion pathways and the diffusion barrier.

Most theoretical studies are based on first-principles study using density functional theory (DFT). Even though DFT can provide accurate energies required for the calculation of the activation barrier, it is computationally expensive. Therefore, such calculations are typically performed with small system sizes containing up to 100 atoms. This introduces a challenge because long-ranged elastic strain effects which are known to significantly modify the diffusion coefficients of Li in Si cannot be studied with small system sizes. We believe that this is a major issue with current DFT-based studies of the Li-Si alloys. Instead we employ a classical interatomic potential so that we can study larger system sizes with lower computational cost. We focus our attention on low Li concentrations in Si. At such concentrations, Si has a diamond cubic structure.

The aim of this work is to theoretically analyse lithium diffusion in crystalline Si by understanding the diffusion mechanism in the presence of bulk strain and the interactions between the Li-Si and Li-Li atoms. In our study, we model the Li-Si, Li-Li and Si-Si interactions using 2NN modified embedded atom method (MEAM) potential. The effect of strain on the lithium diffusion barrier in diamond cubic Si is studied using the climbing image nudged-elastic band (NEB) method. This enables us to determine the role played by bulk strain and by local strain arising from Li atoms in the vicinity of a diffusing Li atom. We show that strain can dramatically affect the Li diffusion constant.

The remainder of the paper has the following structure. In Sec. 2, we describe the implementation of the 2NN MEAM interatomic potential, perform validation of the MEAM potential and describe the climbing-NEB method used to find the minimum energy path between the initial and final position of the Li atoms. In Sec. 3, the results from the NEB calculations for Li diffusion are discussed. Finally, conclusions are presented in Sec. 4.

## 2. Methodology

We have employed the MEAM potential of Ref. [46] for Li-Si alloy. First, we validate the MEAM potential. Next, we briefly describe the NEB method we used for calculating the activation barrier.

### *2.1. Validation of the second nearest neighbour (2NN) Modified embedded atom method (MEAM) potential*

In order to correctly describe Li and Si atomic movements and interactions during lithium insertion we need an interatomic potential that can accurately compute the basic material properties of $Li_xSi$, such as lattice constants, elastic constants and cohesive energies. The MEAM potential [47] is frequently employed for metal systems. The original MEAM potential [47] was an improvement over the EAM potential as angular terms to describe covalent nature of the bonding [48, 49] had been introduced. However, it had certain drawbacks since it predicted that the bcc structure is not the most stable structure for Li, which is incorrect. Lee and co-workers proposed the second nearest neighbour (2NN) MEAM interatomic potential [46] which can better describe the bcc structure.

In MEAM, the total energy E of a system of a single type atoms is given by,

$$E = \sum_i [F_i(\overline{\rho}_i) + \frac{1}{2}\sum_{j\neq i} S_{ij}\phi_{ij}(R_{ij})] \quad (1)$$

where $\overline{\rho}_i$ is the background electron density at site i, $F_i$ is the embedding energy required at site i, $\phi_{ij}$ is pair interaction between atoms i and j at a distance $R_{ij}$ and $S_{ij}$ is the screening factor between atoms i and j. The density

$\overline{\rho}_i$ is given by a linear superposition of spherically averaged atomic electron densities and angular-dependent terms. This angular dependence enables covalently bonded systems Si to be described by the MEAM potential. The embedding function $F_i(\overline{\rho}_i)$ is described by

$$F(\overline{\rho}) = AE_c \frac{\overline{\rho}}{\overline{\rho}_0} \ln \frac{\overline{\rho}}{\overline{\rho}_0} \quad (2)$$

where A is an adjustable parameter, $E_c$ is the cohesive energy and $\overline{\rho}_0$ is the background electron density for the reference structure.

Pure Si has diamond cubic crystal structure with a lattice constant of 5.427 Å [45]. Si retains the cubic structure at very low Li concentrations. The preferred positions for the Li and Si atoms are as follows. A Li atom can be placed in a unit cell of Si crystal at different sites shown in Fig. 1. These include the tetrahedral site ($T_d$), hexagonal site ($H_{ex}$), centre position between a Si-Si bond ($B_c$) and centre of the distance between next nearest silicon neighbours ($C_n$) [45, 50]. In Fig. 1, the orange, green and brown spheres represent the corner, face-centred and tetrahedral positions, respectively, for the Si atoms. Here the red sphere denotes the tetrahedral site (½, ½, ½), the dark blue sphere denotes the hexagonal site (5/8, 5/8, 5/8), the sky blue sphere denotes the bond-centre site (1/8, 1/8, 1/8) and the brown sphere denotes the centre of the distance between next nearest silicon neighbours site (1/4, 1/4, 0).

We tested the MEAM potential by computing the binding energy for Li for different insertion sites. The binding energy per Li atom $E_b(n)$ is calculated as $E_b(n) = [E_{n_{LiSi}} - E_{Si}]/n$ where $E_{n_{LiSi}}$ is the total energy of the system containing n Li atoms and 1728 Si atoms and $E_{Si}$ is the total energy of the bulk Si system with 1728 atoms. A lower value of the binding energy corresponds to an energetically favourable site for Li. A single Li atom was inserted into a 6x6x6 super cell of bulk Si with 1728 Si atoms. Table 1 displays the calculated binding energies for lithium in different sites. From the binding energy listed above it is clearly indicated that the tetrahedral position is the most energetically favourable site. This is in agreement with literature values obtained using DFT [45, 50]. We find that although the MEAM energies are quantitatively not in agreement with DFT, however, MEAM does capture the correct trend for the relative stability of the sites. This indicates that the structure obtained from the MEAM potential will be physically relevant.

We calculated the total energy of a system consisting of 6x6x6 super cell of bulk Si with 1728 Si atoms and different number of Li atoms. The Li atoms were inserted at the tetrahedral sites in same unit cell. It is known that the energy of the system decreases as more Li atoms are inserted, i.e., the insertion of Li is thermodynamically favourable. Fig. 2 shows the total energy of the system decreases when Li occupancy increases. In our study of the activation barrier, we only focus on the cases where either one Li atom or two Li atoms are present. Clearly, we find that the MEAM potential provides the correct behaviour for the Li-Si energies. A stronger test for the energies from the MEAM potential is performed next, where we compute the activation barriers.

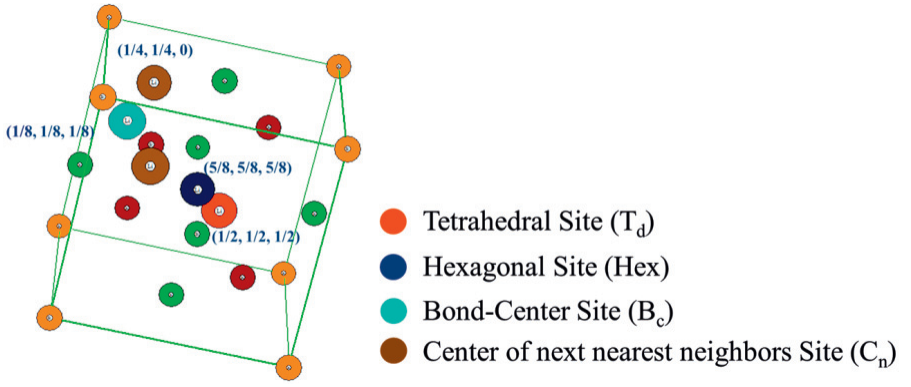


Fig. 1. Insertion sites for Li atoms in a Si unit cell. The positions for the Si atoms are also shown.

Table 1. Binding energies for Li at different sites in bulk Si system in eV using DFT (from Ref.[50]) and MEAM (this work). See Fig. 1 for understanding the notation used in the table for the sites.

| Position | Binding Energy (eV, from Ref.[50]) | Binding Energy (eV, using MEAM) |
|---|---|---|
| $T_d$ | -1.15 | -0.17 |
| $H_{ex}$ | -0.60 | 0.38 |
| $B_c$ | 1.27 | 0.98 |
| $C_n$ | 1.39 | 1.02 |

We also computed the cohesive energy for different Li compositions in the $Li_xSi_y$ system and compared the cohesive energies to value obtained in Ref. [46]. Note that the crystal structure of the Li-Si alloy changes for the compositions that were studied. The lattice constant for the crystal structure was found by obtaining the Murnaghan equation of state. Table 2 shows the lattice constants obtained from the MEAM potential. The cohesive energy for different $Li_xSi_y$ structures from the MEAM potential and from Ref. [46] are also shown. It is evident cohesive energies are very close to each other. This further confirms that the MEAM potential is able to describe the system with reasonable accuracy.

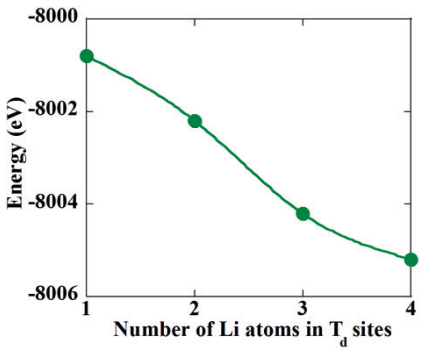


Fig. 2. Total energy is plotted against the number of Li atoms at Tetrahedral (Td) sites in bulk Si system containing 1728 Si atoms. The energy is obtained after performing an energy minimization calculation.

Table 2. Lattice constants and cohesive energies obtained from the MEAM potential for different $Li_xSi_y$ phases.

| $Li_xSi_y$ | a | b | c | $E_c$ (in eV, from Ref. [46]) | $E_c$ (in eV, MEAM) |
|---|---|---|---|---|---|
| $Li_1Si_1$ | 9.356 | 9.356 | 5.742 | 3.301 | 3.19 |
| $Li_{15}Si_4$ | 10.616 | 10.616 | 10.616 | 2.466 | 2.26 |
| $Li_{12}Si_7$ | 8.553 | 19.647 | 14.317 | 2.950 | 2.64 |
| $Li_{13}Si_4$ | 7.993 | 15.103 | 4.427 | 2.412 | 2.22 |

### *2.2. Nudged Elastic Band (NEB) method*

When a Li atom moves from one tetrahedral site to a nearest vacant tetrahedral site it encounters an energy barrier. In our past studies, we have found that the local environment plays an important role in determining the barrier and the rate constant. We expect a similar behaviour here, i.e., we expect that when a Li atom is present in the vicinity of the hopping Li atom, the activation barrier can change. Similarly, the activation barrier can change due to the presence of bulk strain in the material. We have employed the climbing-image Nudged Elastic Band (NEB) method [51] in this work to understand the change in the minimum energy path and activation barrier. The initial and final states are both local minimum in the potential energy surface. We obtain these states by inserting the Li atom(s) in the tetrahedral sites and then perform an energy minimization calculation. The energy minimization is performed using the limited memory BFGS method. In order to perform the NEB calculation, 25 images of the system starting from the initial to the final state are used to find the minimum energy path. A spring constant in the

range of 0.1-1 eV/Å$^2$ is employed. We perform an optimization calculation in which all images, except for the first and last, are simultaneously allowed to relax.

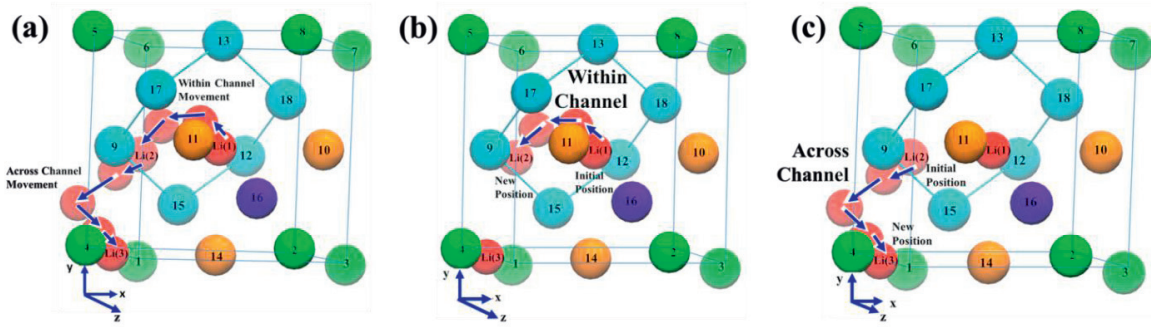


Fig. 3. Schematic showing the hop movement of a Li atom from a tetrahedral site to another tetrahedral site. (a) Only one Li atom present. Hop from site denoted Li(1) to Li(2) through the hexagonal ring in the unit cell (termed as within channel) and hop from site denoted Li(2) to Li(3) (termed as across channel movement of Li atom are shown; (b) Two Li atoms are present. One Li atom hops from site Li(1) to Li(2), while the other Li atom is present at the site Li(3); (c) Two Li atoms are present. One Li atom hops from site Li(2) to Li(3), while the other Li atom is present at the site Li(1).

Fig. 3 shows the types of Li atom movements studied in this work. A single Li atom is allowed to hop from one tetrahedral site to another tetrahedral site. Fig. 3a shows the case where a single Li atom is present in the unit cell. One movement we have studied involved the hopping Li atom to pass through the hexagonal ring in the unit cell (formed by the Si atoms 13, 18, 12, 15, 9 and 17). Such a move is referred to as within channel movement. The movement undertaken by the Li atom is shown by the red sphere as it hops from the site denoted from Li(1) to the site Li(2) is shown. The arrows show how the Li atom hops from one site to the other. The other type of move we have studied involves the Li moving out of the unit cell from site denoted Li(2) to site Li(1). We refer to this move as across channel movement. Fig. 3a also shows other Si atoms in the unit cell which are common to both within and across channel moves. Spheres numbered 1- 8 are corner Si atoms, spheres 9-14 are the face-centered Si atoms, and spheres 15-18 are tetrahedral Si atoms. Fig. 4 shows the energy diagram for the two types of moves when a single Li atom is present. It is observed that the activation energy barrier for the Li hop in both cases is 0.58 eV in the absence of bulk strain. This is in agreement with previous DFT-based barriers (Ref. [50]). We conclude that the MEAM potential is able to obtain the activation barrier reasonably well.

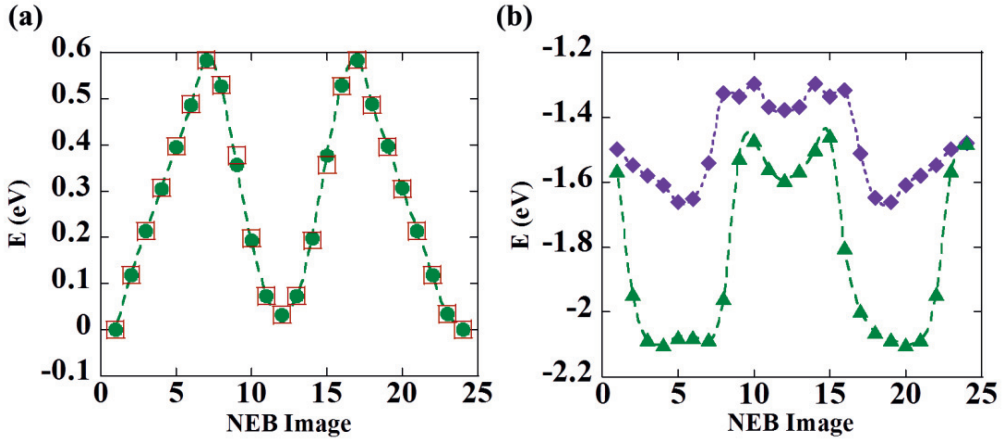


Fig. 4. Energy diagram for Li atom hopping within channel and across channel with 0% biaxial strain. Four cases are shown: (a) circles and squares denote the Li within channel and across channel moves when a single Li atom is present, respectively; while (b) diamonds and triangles denote the Li within and across channel moves two Li atoms are present.

## 3. Results

In this section we discuss the energy diagram and minimum energy path when a single Li atom hops from one tetrahedral site to a nearest vacancy tetrahedral site. The effect of nearby Li atom that is not hopping is studied. Next, we study the role of bulk strain on the activation energy barrier.

### *3.1. Energy diagram and minimum energy path for Li diffusion in bulk Si*

Fig. 3a shows the Li atom hopping within and across the channel when single Li atom is present in the unit cell. It is evident that the Li atom does not move in a straight line from one tetrahedral site to the vacant tetrahedral site. In the case of the within channel move, the Li atom passes through the hexagonal Si ring in the unit cell, reaches the vacant Si tetrahedral position, and then moves towards the vacant Li tetrahedral site. The energy diagram in Fig. 4 shows that there is an intermediate state between the initial and final position. The Li atom situated at the vacant Si tetrahedral position corresponds to the intermediate state. There are two saddle points in the energy diagram. These saddle points correspond to hexagonal sites for Li. The activation barrier is obtained as the difference between the saddle point and the initial state energy. Both within and across channel moves result in a similar energy diagram.

Fig. 3b and c denote the Li atom move in the presence of a second Li atom. In Fig. 3b, the hopping Li atom moves from the site denoted Li(1) to Li(2), i.e., it is a within-channel move, while the second Li atom is present at the site denoted Li(3). In Fig. 3c, the hopping Li atom moves from site denoted Li(2) to Li(3), i.e., it is an across channel move, while the second Li atom is present at site denoted Li(1). The movement of the Li atom is shown by arrows in Fig. 3b and c. It is observed that once again the minimum energy pathway passes through $T_d$-Hex-$T_d$ sites. However, the energy diagrams for these moves shown in Fig. 4 clearly demonstrate that there is an effect of the nearby Li atom. We find that the energy of the initial state of the system is lower when two Li atoms are present than the energy for the single Li atom (as mentioned earlier). Interestingly, it appears that the presence of the second Li atom introduces new energy basins in the potential energy surface. For instance, we find that the NEB images 2-8 and 18-24 for the across channel move have an energy lower than the initial and final state. A small barrier is present as the system moves from NEB image 1 to 2. The intermediate state is still present along the minimum energy path. The intermediate state energy is close to the initial and final state energy. A similar behaviour is observed for within channel moves. We attribute this change in the energy diagram to the opening-up of the Si hexagon ring when the second Li atom is present. This allows the hopping Li atom to relax to a lower energy state. Furthermore, the saddle points are not as high as in the single Li atom case (within channel move). The difference in the within and across channel moves are attributed to the way the hexagonal ring is oriented with respect to the second Li atom. The activation barrier is computed from the saddle point energy in and the lowest energy in the energy diagram. We find that the activation energy barrier is 0.175 eV in the absence of bulk strain for Li diffusion within channel in presence of a second Li atom. This corresponds to a low barrier atomic move. For Li diffusion across channel in presence of another Li atom, the activation energy barrier is found to be 0.65 eV at zero strain. Clearly, the direction and local environment of the hopping Li atom strongly influences the activation barrier.

### *3.2. Effect of bulk strain on activation energy*

We repeated the same calculation discussed in Sec. 3.1 using different biaxial strains namely -2,-1, 1 and 2%. The Poisson ratio for Si used in our calculation is 0.34. This value of the Poisson ratio is close to the experimental value of 0.28 for Si.

Fig. 5 a-c shows the energy diagram for the Li atom hop with channel when a single Li atom is present. It is observed that the energy of the system increases as the strain increases. Similar behaviour is observed with a Li atom hop across channel (shown Fig. 5 d-f). The activation barrier obtained from Fig. 5 is plotted in Fig. 6 in terms of the strain. It is observed that the activation barrier is lowered by as much as 0.05 eV when a -2% biaxial strain is present. The activation barrier increases as the strain increases to 0%. The activation barrier decreases as the strain increases to 2%. The movement of the Li atom is complicated by the relaxation atoms in the vicinity. Consequently, it is not straightforward to identify the role played by the various Si-Si bonds in the local environment of the hopping Li atom. We believe that as the Li atom moves within channel from its initial state, the largest change in the energy arises from the interaction between the Li atom and the Si atoms 9, 17, 12 and 15. In particular, we observe visually that the bonds between atoms 9-17 and 12-18 in Fig. 3 are stretched at the saddle point. At -2% strain, these

bonds are compressed. However, at the saddle point the presence of Li causes the bond to stretch closer to the equilibrium Si-Si bond length. Even though the compressive biaxial strain increases the overall energy of the system, the saddle point energy is lowered to some extent because of this fact. Hence, we find that the activation barrier increases as the strain increases from -2 to 0%. When a tensile biaxial strain is applied, there is more room for the Li atom to move. The saddle point energy is somewhat lowered because of this, even though the bulk strain will lead to an overall increase in the system energy. Hence, we find that the activation barrier decreases as the strain increases from 0 to 2%. Similar arguments can explain the behaviour observed with the across channel move.

We obtain the rate constant for a process at different strain from Arrhenius rate expression $k = \upsilon \exp(-E_a / k_B T)$ where $\upsilon$ is the pre-exponential factor, $E_a$ is the activation energy barrier, T is the system temperature and $k_B$ is the Boltzmann constant. Assuming the pre-exponential factor to be $10^{13}$ $sec^{-1}$ and temperature is 300K, we find that for 0% strain and an activation barrier of 0.58eV, the rate is $1.8 \times 10^{3}$ $sec^{-1}$. For 1% strain, activation energy barrier is 0.54 eV, the rate of the process increases by almost 4 times to $8.5 \times 10^{3}$ $sec^{-1}$. It is interesting to note that when the barrier is 0.175 eV (as shown in Fig. 4) the rate constant can be as large as $1.1 \times 10^{10}$ $s^{-1}$. Such a large change in the rate constant can dramatically affect the diffusion constant.

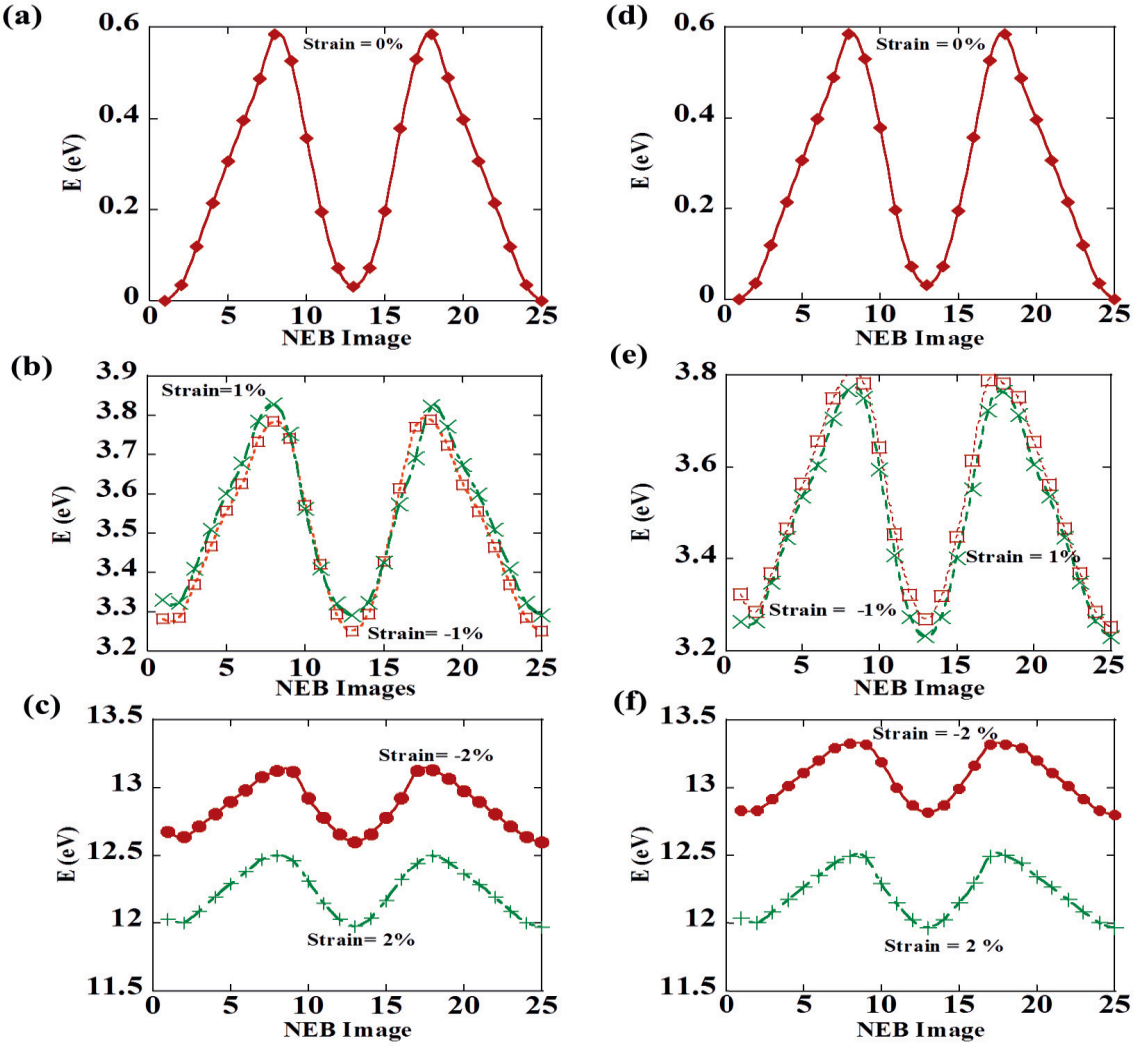


Fig. 5. Energy diagram for single Li atom hopping a-c) within channel and d-f) across channel in the presence of different values of biaxial strain.

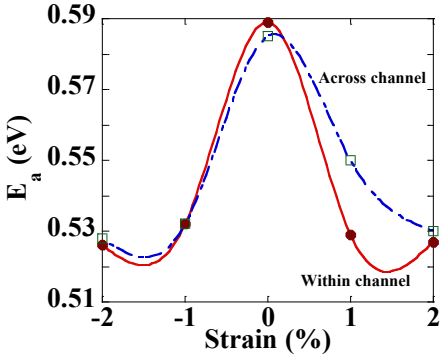


Fig. 6. The activation barrier for Li hopping $E_a$ is plotted against the biaxial strain for single Li atom hopping within channel and across channel.

### *3.3. Effect of strain on Si- Si bond-length during Li diffusion in bulk Si*

The presence of Li atom creates local strain in the system. We find that Si-Si bonds between atoms 9, 12 and 15 in Fig. 3 are either compressed or stretched by a large amount to allow the Li atom to move from its initial state to final state during within channel movement. Initially when Li atom is at initial state for within channel movement, the two Si-Si bonds far from the lithium atom have bond-length of 2.45 Å [50]. Due to presence of Li atom in the local environment, the 9-15 and 15-12 Si-Si bonds are initially stretched and then later compressed. As Si-Si bonds are stretched, the activation energy barrier also changes. The same behaviour is observed during Li hopping across the channel. We believe that the change in energy along the minimum energy path is primarily due to the stretching or compression of the bonds.

## 4. Conclusions

Nudged elastic band calculations for Li atom hop from a Li tetrahedral site to a nearest vacancy tetrahedral site were performed in the presence of bulk strain as well as local strain arising from the presence of a nearest neighbour Li atom. We find that the presence of a nearby Li atom can dramatically change the activation barrier and the rate constant. In comparison, the effect of bulk strain is to change the activation barrier by as much as 0.05 eV. This will result in a change in rate constant by a factor of 10. Thus we conclude that kinetic models that capture the effect of both bulk and local strain need to be developed so that the insertion and removal of Li in Si can be accurately predicted.

## Acknowledgements

AC acknowledges the support of BRNS Young Scientist Award from the Department of Atomic Energy (DAE-BRNS) No. 2011/36/43-BRNS/1975.

## References:

[1] Bauer P. Batteries for space power systems ( NASA SP-172). National Aeronautics Scientific and Technical Information Division; 1968.
[2] Yoshio M, Brodd RJ, Kozawa A. Lithium-ion batteries: science and technologies. Springer; 2009.
[3] Beaulieu LY, Eberman KW, Turner RL, Krause LJ, Dahn JR. Colossal reversible volume changes in lithium alloys. Electrochem. Solid-State Lett. 2001; 4: A137–A140.
[4] Hatchard TD, Dahn JR. In situ XRD and electrochemical study of the reaction of lithium with amorphous silicon. J. Electrochem. Soc. 2004; 151: A838-A842.
[5] Deshpande R, Cheng YT, Verbrugge MW. Modeling diffusion-induced stress in nanowire electrode structures. J. Power Sources 2010; 195: 5081–5088.
[6] Verbrugge MW, Cheng YT. Stress and strain-energy distributions within diffusion-controlled insertion-electrode particles subjected to periodic potential excitations. J. Electrochem. Soc. 2009; 156: A927-A937
[7] Kasavajjula U, Wang C, Appleby AJ. Nano- and bulk-silicon-based insertion anodes for lithium-ion secondary cells. J. Power Sources 2007; 163: 1003-1039.

[8] Aurbach D. Review of selected electrode–solution interactions which determine the performance of Li and Li ion batteries. J. Power Sources 2000; 89: 206-218.
[9] Kim H, Seo M, Park MH, Cho J. A critical size of silicon nano-anodes for lithium rechargeable batteries. Angewandte Chemie. 2010; 49: 2146–2149.
[10] Chan CK, Peng H, Liu G, McIlwrath K, Zhang XF, Huggins RA, Cui Y. High-performance lithium battery anodes using silicon nanowires. Nature Nanotechnology 2008; 3: 31-35.
[11] Park MH, Kim MG, Joo J, Kim K, Kim J, Ahn S, Cui Y, Cho J. Silicon nanotube battery anodes. Nano Lett. 2009; 9: 3844–3847.
[12] Cui LF, Ruffo R, Chan CK, Peng H, Cui Y. Crystalline-amorphous core−shell silicon nanowires for high capacity and high current battery electrodes. Nano Lett. 2009; 9: 491–495
[13] Cui LF, Yang Y, Hsu CM, Cui Y. Carbon−silicon core−shell nanowires as high capacity electrode for lithium ion batteries. Nano Lett. 2009; 9: 3370–3374.
[14] Kim H, Han B, Choo J, Cho J. Three-dimensional porous silicon particles for use in high-performance lithium secondary batteries. Angewandte Chemie. 2008; 47: 10151–10154.
[15] Yao Y, McDowell MT, Ryu I, Wu H, Liu N, Hu L, Nix WD, Cui Y. Interconnected silicon hollow nanospheres for lithium-ion battery anodes with long cycle life. Nano Lett. 2011; 11: 2949–2954.
[16] Magasinski A, Dixon P, Hertzberg B, Kvit A, Ayala J, Yushin G. High-performance lithium-ion anodes using a hierarchical bottom-up approach. Nature Mater. 2010; 9: 353–358.
[17] Liu N, Wu H, McDowell MT, Yao Y, Wang C, Cui Y. A yolk-shell design for stabilized and scalable Li-ion battery alloy anodes. Nano Lett. 2012; 12: 3315–3321.
[18] Read AJ, Needs RJ, Nash KJ, Canham LT, Calcott PDJ, Qteish A. First-principles calculations of the electronic properties of silicon quantum wires. Phys. Rev. Lett. 1992; 69: 1232-1235.
[19] Niquet YM, Lherbier A, Quang NH, Fernández-Serra MV, Blase X, Delerue C. Electronic structure of semiconductor nanowires. Phys. Rev. B 2006; 73: 165319.
[20] Sacconi F, Persson MP, Povolotskyi M, Latessa L, Pecchia A, Gagliardi A, Balint A, Fraunheim T, Carlo AD. Electronic and transport properties of silicon nanowires. J. Comput. Electron. 2007; 6: 329-333.
[21] Leão CR, Fazzio A, Silva AJR. Si nanowires as sensors: choosing the right surface. Nano Lett. 2007; 7: 1172–1177.
[22] Xu X, Servati P. Facet-dependent electronic properties of hexagonal silicon nanowires under progressive hydroxylation and surface reconstruction. Nano Lett. 2009; 9: 1999–2004.
[23] Christensen J, Newman J. Stress generation and fracture in lithium insertion materials. J. Solid State Electrochem. 2006; 10: 293-319.
[24] Cheng YT, Verbrugge MW. Diffusion-induced stress, interfacial charge transfer, and criteria for avoiding crack initiation of electrode particles. J. Electrochem. Soc. 2010; 157: A508-A516.
[25] Christensen J. Modeling diffusion-induced stress in Li-ion cells with porous electrodes. J. Electrochem. Soc. 2010; 157: A366-A380
[26] Christensen J, Newman J. A mathematical model of stress generation and fracture in lithium manganese oxide. J. Electrochem. Soc. 2006; 153: A1019-A1030.
[27] Golmon S, Maute K, Dunn ML. Numerical modeling of electrochemical–mechanical interactions in lithium polymer batteries. Computers & Structures 2009; 87: 1567–1579.
[28] Bhandakkar TK, Gao H. Cohesive modeling of crack nucleation under diffusion induced stresses in a thin strip: Implications on the critical size for flaw tolerant battery electrodes. Int. J. Solids Struct. 2010; 47: 1424–1434.
[29] Yang F. Effect of local solid reaction on diffusion-induced stress. J. Appl. Phys. 2010; 107: 103516.
[30] Cheng YT, Verbrugge MW. The influence of surface mechanics on diffusion induced stresses within spherical nanoparticles. J. Appl. Phys. 2008; 104: 083521.
[31] Haftbaradaran H, Gao H, Curtin WA. A surface locking instability for atomic intercalation into a solid electrode. Appl. Phys. Lett. 2010; 96: 091909.
[32] Kang YM, Suh SB, Kim YS. First-principle calculation-assisted structural study on the nanoscale phase transition of Si for Li-ion secondary batteries. Inorg. Chem. 2009; 48: 11631–11635.
[33] Shenoy VB, Johari P, Qi Y. Elastic softening of amorphous and crystalline Li–Si phases with increasing Li concentration: a first-principles study. J. Power Sources 2010; 195: 6825–6830.
[34] Limthongkul P, Jang YI, Dudney N J., Chiang YM. Electrochemically-driven solid-state amorphization in lithium-silicon alloys and implications for lithium storage. Acta Mater. 2003; 51: 1103-1113.
[35] Chevrier VL, Zwanziger JW, Dahn JR. First principles studies of silicon as a negative electrode material for lithium-ion batteries. Can. J. Phys. 2009; 87: 625-632.
[36] Li J, Dahn JR. An in situ x-ray diffraction study of the reaction of Li with crystalline Si. J. Electrochem. Soc. 2007; 154: A156-A161.
[37] Obrovacz MN, Christensen L. Structural changes in silicon anodes during lithium insertion/extraction. Electrochem. Solid-State Lett. 2004; 7: A93-A96.
[38] Guo H, Zhao H, Yin C, Qiu W. A nanosized silicon thin film as high capacity anode material for Li-ion rechargeable batteries. Mat. Sci. Eng. B-Solid 2006; 131: 173–176.
[39] Chan CK, Ruffo R, Hong SS, Huggins RA, Cui Y. Structural and electrochemical study of the reaction of lithium with silicon nanowires. J. Power Sources 2009; 189: 34-39.
[40] Laïk B, Eude L, Ramos JPP, Cojocaru CS, Pribat D, Rouvière E. Silicon nanowires as negative electrode for lithium-ion microbatteries. Electrochim. Acta 2008; 53: 5528–5532.
[41] Ma H, Cheng F, Chen JY., Zhao JZ, Li CS, Tao ZL, Liang J. Nest-like silicon nanospheres for high-capacity lithium storage. Adv. Mater. 2007; 19: 4067–4070.
[42] Yang Y, McDowell MT, Jackson A, Cha JJ, Hong SS, Cui Y. New nanostructured $Li_2S$/Silicon rechargeable battery with high specific energy. Nano Lett. 2010; 10: 1486–1491.
[43] Ruffo R, Hong SS, Chan CK, Huggins RA, Cui Y. Impedance analysis of silicon nanowire lithium ion battery anodes. J. Phys. Chem. C 2009; 113: 11390–11398.

[44] Cho J. Porous Si anode materials for lithium rechargeable batteries. J. Mater. Chem. 2010; 20: 4009-4014.
[45] Wan W, Zhang Q, Cui Y, Wang E. First principles study of lithium insertion in bulk silicon J. Phys.: Condens. Matter 2010; 22: 415501.
[46] Cui Z, Gao F, Cui Z, Qu J. A second nearest-neighbor embedded atom method interatomic potential for Li–Si alloys. J. Power Sources 2012; 207: 150–159.
[47] Lee BJ, Baskes MI, Kim H, Cho YK. Second nearest-neighbor modified embedded atom method potentials for bcc transition metals. Phys. Rev. B 2001; 64: 184102.
[48] Baskes MI. Modified embedded-atom potentials for cubic materials and impurities. Phys. Rev. B 1992; 46: 2727-2742.
[49] Kubota Y, Escaño MCS, Nakanishi H, Kasai H. Electronic structure of Li-Si. J. Alloy Compd. 2008; 458: 151–157.
[50] Zhao K, Wang WL, Gregoire J, Pharr M, Suo Z, Vlassak JJ, Kaxiras E. Lithium-assisted plastic deformation of silicon electrodes in lithium-ion batteries: a first-principles theoretical study. Nano Lett. 2011; 11: 2962–2967.
[51] Henkelman G, Jónsson H. Improved tangent estimate in the nudged elastic band method for finding minimum energy paths and saddle points. J. Chem. Phys. 2000; 113: 9978-9985.